Indian Journal of Pure & Applied Physics
Vol. 56, February 2018, pp. 128-135

Structural analysis and theoretical investigations in Pb additive Se-Te-Ge chalcogenide nano-composites

Neha Sharma[a], Balbir Singh Patial[b]*& Nagesh Thakur[a]

[a]Department of Physics, H P University, Shimla 171 005, India
[b]Department of Physics, Government College Sunni, Shimla 171 301, India

Received 22 May 2017; accepted 3 November 2017

In the present study, the impact of lead addition on the structural and physical properties of newly prepared quaternary $(Se_{80}Te_{20})_{94-x}Ge_6Pb_x$ (x= 0, 2, 4, 6, 8 and 10) chalcogenide nano–composites has been studied in detail. Nano particle size of each Pb addtive chalcogenide alloy has been deduced using the highest intensity peak of the X-ray diffractograms and it has also been confirmed by field emission scanning electron microscope (FESEM). The detailed study of physical parameters namely average co-ordination number (Z) and number of constraints, lone pair electrons, glass transition temperature, heat of atomization, cohesive energy and energy gap has been made. It is observed that Z and constraints have been found to increase with the addition in Pb content. However, all the other investigated parameters viz lone pair electrons, glass transition temperature, heat of atomization, cohesive energy and energy gap show a reverse variation. Glass transition temperature has been estimated theoretically using Tichy-Ticha approach and found to be in consonance with the experimental results. The cohesive energy has been calculated using chemical bond approach (CBA) model. Due to lower band gap of Pb, the overall bandgap of the composition has been found to decrease with Pb at.wt.%.

Keywords: Chalcogenide nano-composites, Glass transition temperature, Heat of atomization, Mean bond energy, Cohesive energy, Energy gap

1 Introduction

Chalcogenide nano-particles show dramatic changes in their structural, optical and electrical characteristics due to their size dependent properties. It also provides new physical and chemical properties with their applications in optical recording, optical imaging and microelectronics. Formation of nanostructure in chalcogenides becomes an interesting topic and studies in this field are still at the starting point as all the features have not been brought to the light. So there is a lot of scope for the study of these materials in a nanometric range[1-4].

Se-Te based systems are preferred because they have greater hardness, higher crystallization temperature, higher photosensitivity and smaller ageing effects. Also Se-Te alloys improve the corrosion resistance and optical sensitivity[5]. Addition of Ge as third element to the Se-Te system increases the contribution to long term room temperature and degree of cross-linking. It is known that binary and ternary chalcogenides have some drawbacks. In the present system, we have chosen Pb as an additive element as lead chalcogenide is the only basic material of modern infrared optoelectronics. Addition of lead metallic elemental impurities to the bulk Se-Te-Ge system increases the conductivity and can also cause p to n-type transition. Pb atom is heavy due to which it provides compactness to the system. Now day's attention is extended over quaternary systems for optoelectronic applications[6-9].

In the present work, newly formulated quaternary $(Se_{80}Te_{20})_{94-x}Ge_6Pb_x$ (x = 0, 2, 4, 6, 8 and 10) chalcogenide nano-composites were prepared using melt-quench technique. The structural characteristics, i.e., nano-particle size were derived using X-ray diffraction (XRD) and field emission scanning electron microscope (FESEM). The physical parameters namely average coordination number, lone pair electrons, number of constraints, fraction of floppy modes, glass transition temperature, heat of atomization, mean bond energy, energy gap and cohesive energy were deduced using different approaches and their composition dependence was discussed in detail.

2 Experimental Details

The bulk $(Se_{80}Te_{20})_{94-x}Ge_6Pb_x$ (x = 0, 2, 4, 6, 8 and 10) chalcogenide alloys were prepared using melt

*Corresponding author (E-mail: bspatial@gmail.com)

quenching technique. 5N highly pure materials (99.999%) were weighed according to their atomic percentages with an accuracy of 10^{-4} g and sealed in a quartz ampoule under a vacuum of ~10^{-5} torr. The sealed ampoules were then placed in a furnace for 10 h, where the temperature was raised up to 1000 °C to make the melt homogeneous. The quenching was done in the ice cold water rapidly. Structural characterization was done using XRD technique and FESEM. For these characterizations, bulk sample of the investigated composition was crushed into a very fine powder. XRD analysis was carried out with the help of Analytical X'Pert-Pro diffractometer (PW 3050/60) in the range 10°<2θ<90° at a scanning rate of 1°/min equipped with a nickel filter using Cu target source (λ = 1.5483 Å). Figure 1 shows the XRD pattern of all the investigated alloys. The XRD sepectrum of $(Se_{80}Te_{20})_{94}Ge_6$ confirms the amorphous nature of the ternary parent alloy as no prominent peak was observed. However, the XRD spectra of Pb additive quaternary $(Se_{80}Te_{20})_{94-x}Ge_6Pb_x$ (x = 2, 4, 6, 8 and 10) alloys were found to associate with sharp peaks. The average particle size (D) was deduced from the highest peak intensity in the spectrum by using the Scherrer formula:

$$D = K\lambda/\beta\theta \quad \ldots (1)$$

where K is the Scherrer constant (K = 0.9), λ is the wavelength (1.5483 Å), β is the full width at half the maximum (FWHM) in radiation of x-ray diffraction peak and θ is the Bragg's angle (degree) at peak position. It was observed that the crystalline size of all the investigated Pb additive chalcogenide bulk alloys lie in nano range between 20 and 80 nm (Table 1). However, other sharp characteristic peaks (with less intensity than the highest intense peak) were also observed with the addition of Pb to the parent alloy. Thus, Pb might be compensating disorder of lower concentrations. Since reduction in disorder always leads to most stable state, as a result, the resulting composition is more stable[10]. The deduced range of the average nano range particle size of the quaternary bulk alloys was further confirmed by FESEM. FESEM correlates the surface appearance with surface morphology. It also characterizes the size and also analyses the defects. Figure 2 shows the surface morphology for investigated quaternary $(Se_{80}Te_{20})_{94-x}Ge_6Pb_x$ (x = 0, 2, 4, 6, 8 and 10) alloys using FESEM.

The thermal behaviour of these studied nano-composites was investigated using differential scanning calorimetry (DSC) technique. About 3-5 mg of sample in powder form was encased in the aluminium pan and values of different characteristics; glass transition temperature, crystallization temperature and melting

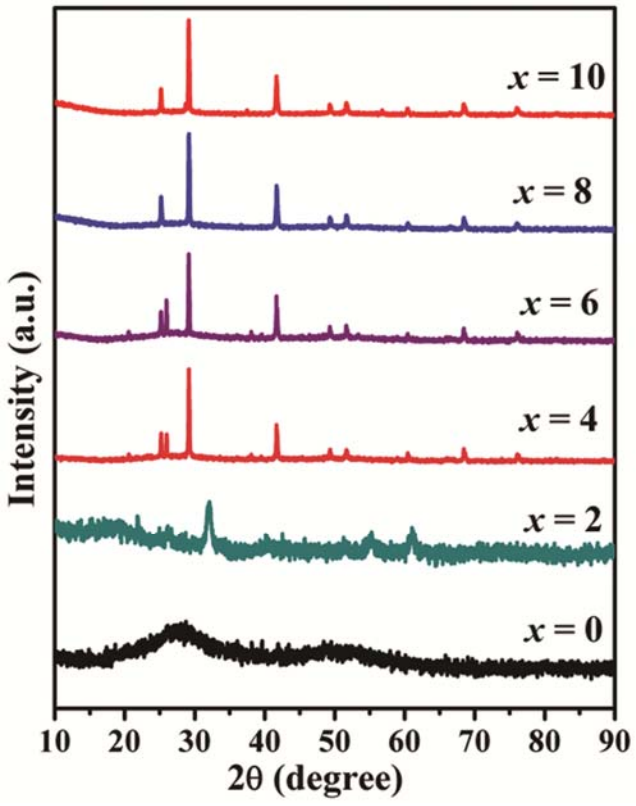

Fig. 1 — X-ray diffraction pattern of the chalcogenide $(Se_{80}Te_{20})_{94-x}Ge_6Pb_x$ (x = 0, 2, 4, 6, 8 and 10) nano-composites.

Table 1 — Values of average particle size, average co-ordination number, number of constraints, lone-pair electrons, fraction of floppy modes and deviation from the stoichiometry for $(Se_{80}Te_{20})_{94-x}Ge_6Pb_x$ (x = 0, 2, 4, 6, 8 and 10) alloys.

Composition	D (nm)	Z	N_c	L	f	R
$(Se_{80}Te_{20})_{94}Ge_6$	-	2.12	2.30	3.76	0.23	7.83
$(Se_{80}Te_{20})_{92}Ge_6Pb_2$	47.28	2.16	2.40	3.68	0.20	5.75
$(Se_{80}Te_{20})_{90}Ge_6Pb_4$	57.24	2.20	2.50	3.60	0.17	4.50
$(Se_{80}Te_{20})_{88}Ge_6Pb_6$	28.29	2.24	2.60	3.52	0.13	3.66
$(Se_{80}Te_{20})_{86}Ge_6Pb_8$	28.25	2.28	2.70	3.44	0.10	3.07
$(Se_{80}Te_{20})_{84}Ge_6Pb_{10}$	52.05	2.32	2.80	3.36	0.06	2.63

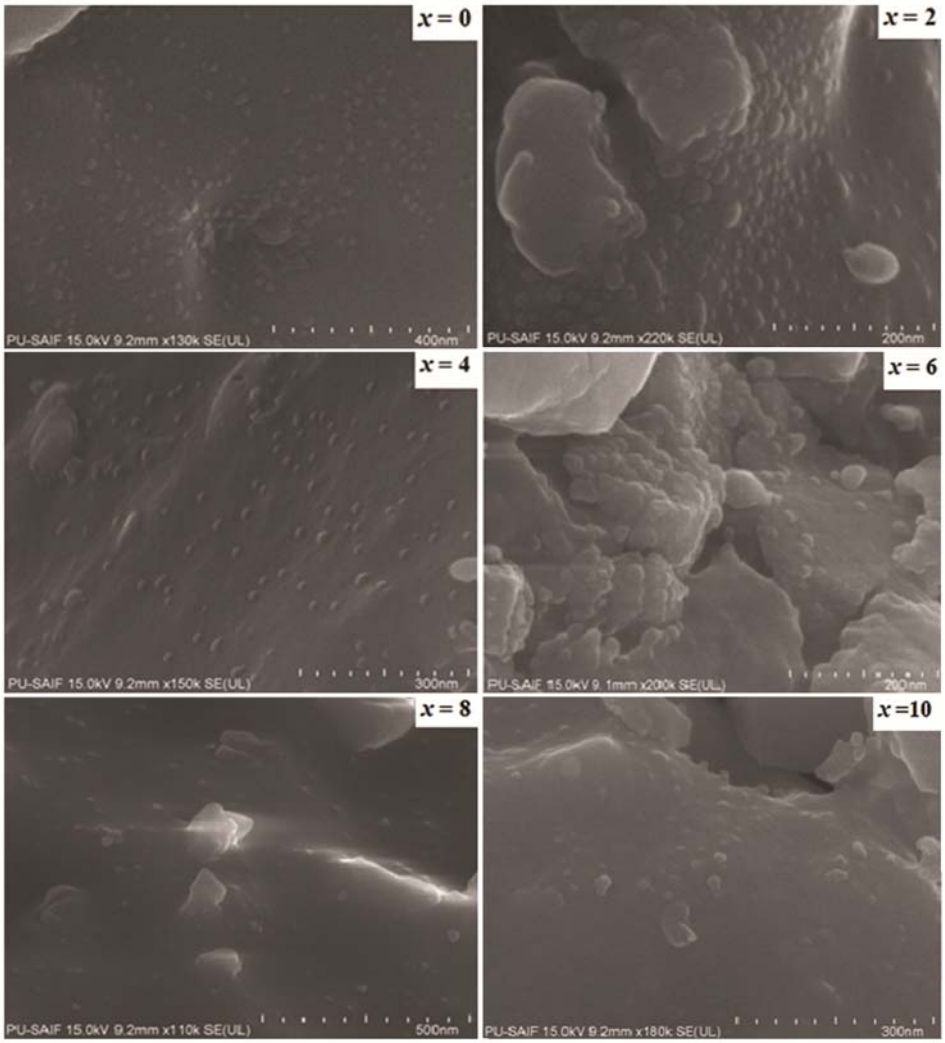

Fig. 2 — FESEM micrographs of $(Se_{80}Te_{20})_{94-x}Ge_6Pb_x$ (x = 0, 2, 4, 6, 8 and 10) nano-composites showing the surface morphology.

temperature were observed at four different heating rates (5, 10, 15 and 20 °C/min).

3 Results and Discussion

3.1 Average co-ordination number and constraints

The average co-ordination number has an immense importance in determining the structure and strength of the material. The average co-ordination number for the quaternary $Se_\alpha Te_\beta Ge_\gamma Pb_\delta$ system is given by[11]:

$$Z = (\alpha Z_{Se}+\beta Z_{Te}+\gamma Z_{Ge}+\delta Z_{Pb})/(\alpha+\beta+\gamma+\delta) \quad \ldots (2)$$

where α, β, γ and δ are the atomic % of Se, Te, Ge and Pb, respectively, and Z_{Se} = 2, Z_{Te} = 2, Z_{Ge} = 4 and Z_{Pb} = 4 are their respective coordination numbers. The deduced values of the average co-ordination number are given in Table 1. Figure 3 shows the variation of Z with Pb at.wt.% and is found to increase with the increase in Pb content. The increase in Z is attributed to the increase in the degree of cross-linking, network rigidity, strength and density between the atoms. The addition of four-fold coordinated lead atom to the two-fold coordinated Se atom increases the mean coordination number. According to Thorpe[12], for mean coordination number <2.4, the system is under coordinated (floppy) whereas for mean coordination number >2.4, network is over constrained (rigid). The floppy to rigid transformation takes place at mean coordination number Z=2.4. In present study, Z <2.4 for all the investigated alloys indicates that the system is floppy type. Moreover, Phillips-Thorpe approach is based on comparing the number of atomic degrees of freedom (N_d) with the number of interatomic force field constraints (N_c) indicates that if N_d<N_c, the network becomes over constrained and stressed-rigid

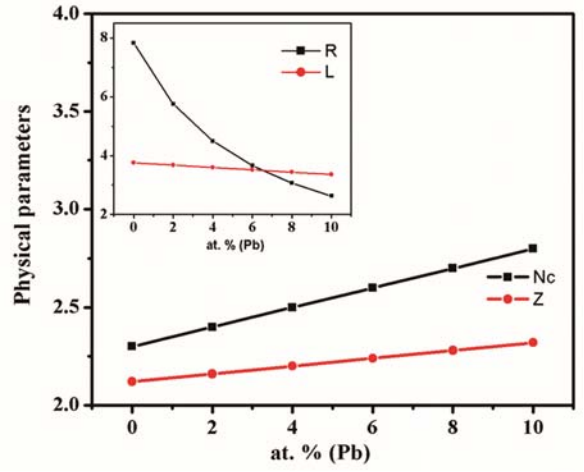

Fig. 3 — Variation of Z, N_c and R, L (inset) with Pb at.wt.%.

structures will percolate through the entire network. If $N_d > N_c$, the network is floppy type. Thus, glass forming tendency would be maximum when number of constraints is equal to the number of degrees of freedom and no stress is present in the system ($N_d = N_c$). There are two types of near-neighbour bonding forces in covalent solids[13]; the bond-stretching ($N_a = Z/2$) and the bond-bending ($N_b = 2Z-3$). The bond-bending constraints come due to angular forces and the bond-stretching constraints are due to radial forces. Therefore, the total numbers of constraints are given by:

$$N_c = N_a + N_b \quad \ldots (3)$$

The deduced values of N_c are given in Table 1 and are found to increase with increasing Pb content. Figure 3 indicates that number of constraints acting on the network is balanced by the number of degrees of freedom available from the atoms in the network. This implies that the increase of Pb to the system makes it more rigid.

3.2 Deviation from the stoichiometry

The parameter stoichiometry (R) determines the deviation from stoichiometry and is defined as the ratio of covalent bond possibilities of chalcogen atoms to that of non-chalcogen atoms. The analysis of R for any chalcogenide system indicates that[14]:

(i) For $R>1$, the system is chalcogen rich, i.e., only heteropolar bonds and chalcogen-chalcogen bonds are present.

(ii) For $R<1$, the system is chalcogen poor and only heteropolar bonds and metal-metal bonds are present.

(iii) For $R=1$, the system reaches the stoichiometric composition since this is a point of existence of only heteropolar bonds.

For the present chalcogen rich system, the quantity R is deduced using the following expression:

$$R = (\alpha Z_{Se} + \beta Z_{Te})/(\gamma Z_{Ge} + \delta Z_{Pb}) \quad \ldots (4)$$

The calculated values of R for each composition are listed in Table 1 and its variation with Pb at.wt.% is shown in Fig. 3. The obtained values of R are greater than one ($R>1$) confirms that the system under investigation is chalcogen rich.

3.3 Role of lone pair electrons in glass forming ability

Two types of interatomic forces occurred in chalcogenide glassy alloys; forces due to short range bonding interactions and forces due to interaction between lone pair electrons. The first one is explained by valence force field whereas the second one needs special contemplation. For shorter distances, the interatomic forces are repulsive. Every chalcogen has a lone pair of electrons. The repulsive lone pair electrons caused steric hurdle and also used to explain the distance of minimum approach. For larger distances, the force is attractive and is accountable for the formation of chalcogenide glasses. The number of lone pair electrons is calculated by using the model proposed by Phillips[15]:

$$L = V - Z \quad \ldots (5)$$

where V and Z are the valance electrons and average co-ordination number, respectively. Zhenhua suggested a criterion for binary and ternary system[16]. For binary system, the number of lone pair electrons must be greater than 2.6 while for the ternary system; it must be greater than 1. For the present investigated system, the number of lone pair electrons goes on decreasing with increasing Pb content and calculated values are given in Table 1. This is due to the interaction between the Pb ion and lone pair electrons of the bridging Se atom. The system with large number of lone pair electrons represents a stable state, specified by flexibility and will favor the glass formation by reducing the strain energy. Figure 3 shows the variation of L with Pb at.wt.%.

3.4 Fraction of floppy modes

The fraction of floppy modes is linked with average co-ordination number Z by the relation:

$$f = 2 - 5Z/6 \quad \ldots (6)$$

According to Thorpe[12], the system should contain $Z < 2.4$ for floppy mode and $Z > 2.4$ for rigid regions in the range of the glass-forming composition. According to Phillips and Thorpe[15], the best suitable condition for glass formation is when $N_c = N_d$. The values of fraction of floppy modes are given in Table 1 and it is clear that fraction of floppy modes decrease with the increase in average co-ordination number. It shows that with the increase in Pb content, the system shifted towards more rigidness as discussed earlier.

3.5 Mean bond energy and glass transition temperature

Mean bond energy $\langle E \rangle$ is an important factor which depends upon many factors, i.e., average co-ordination number, degree of cross-linking, type of bonds and bond energy of the system. According to Tichy-Ticha[17], the mean bond energy for the chalcogen rich system is given by:

$$\langle E \rangle = E_c + E_{rm} \quad \ldots (7)$$

where E_c is the overall contribution to the bond energy arising from strong heteropolar bonds and is given by:

$$E_c = P_r D_{hb} \quad \ldots (8)$$

P_r and D_{hb} is the degree of cross-linking and average heteropolar bond energy, respectively.

E_{rm} is the average bond energy per atom of the remaining matrix and is given as:

$$E_{rm} = (2[0.5Z - P_r] E_{Se\text{-}Se})/Z \quad \ldots (9)$$

where $E_{Se\text{-}Se}$ is the homopolar bond energy of Se-Se atoms. The glass transition temperature for chalcogenide glasses is an important parameter to decide their utility for the specific technological applications[18]. As stated by Tichy-Ticha[19], glass transition temperature (T_g) is related to the mean bond energy and is given by:

$$T_g = 311\ [\langle E \rangle - 0.9] \quad \ldots (10)$$

where T_g is in kelvin and $\langle E \rangle$ is in eV/atom. The mean bond energy values have been used for the prediction of glass transition temperature as T_g is directly proportional to $\langle E \rangle$. Figure 4 shows the DSC thermo grams at heating rate 10 °C/min. The variation of glass transition temperature and mean bond energy in accordance with the variation of lead percentages have been plotted in Fig. 5 and found that both the factors decrease with the increase in lead. The theoretically estimated T_g using Tichy-Ticha approach and experimental values from DSC data are given in Table 2 and we found that they are in consonance with each other.

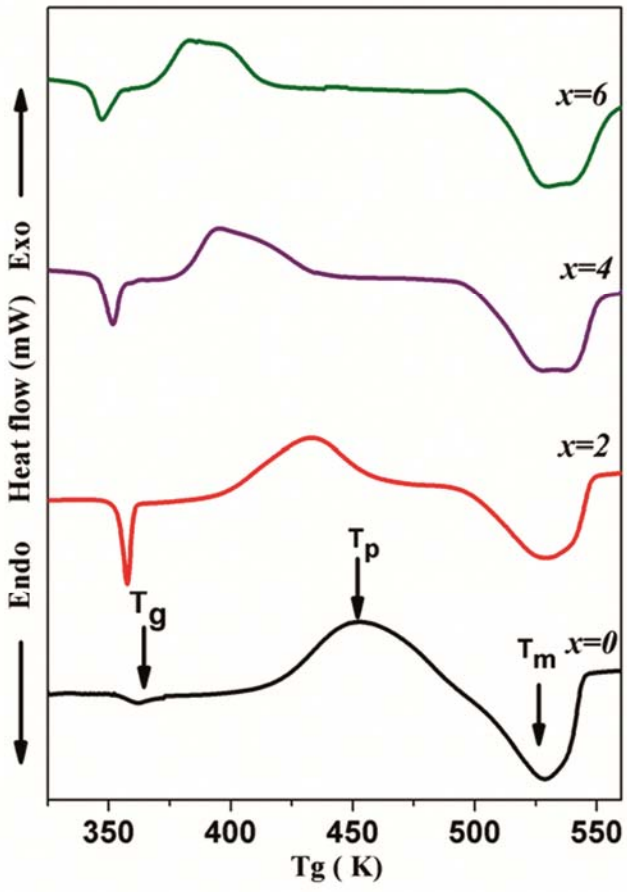

Fig. 4 — DSC thermogram of the $(Se_{80}Te_{20})_{94-x}Ge_6Pb_x$ (x = 0, 2, 4 and 6) composition at heating rate of 10 °C/min.

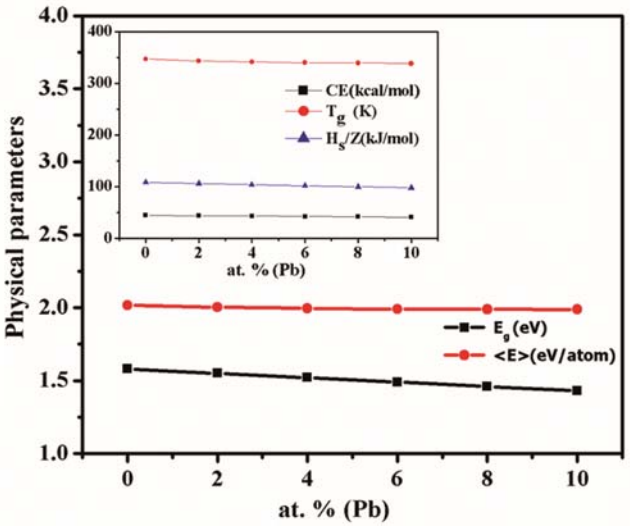

Fig. 5 — Variation of $\langle E \rangle$, E_g and CE, T_g, H_s/Z (inset) with Pb at.wt.%.

3.6 Heat of atomization, cohesive energy and energy gap

Heat of atomization H_s measures the relative bond strength. For the present investigated system heat of atomization is given by[20]:

$$H_s = (\alpha H_s^{Se} + \beta H_s^{Te} + \gamma H_s^{Ge} + \delta H_s^{Pb})/(\alpha+\beta+\gamma+\delta) \quad \ldots (11)$$

The heat of atomization (H_s) value for Se, Te, Ge and Pb are 227 kJ/mol, 197 kJ/mol, 377 kJ/mol and 195 kJ/mol, respectively[20]. The calculated values of heat of atomization (H_s) and average single bond energy (H_s/Z) are given in Table 2. It is observed that H_s and H_s/Z decrease with the increase in Pb content. Average single bond energy (H_s/Z) measures the cohesive energy. The decrease in average bond energy also causes a decrease in the band gap. This is due to increase in the number of Se-Pb bonds (31.47 kcal/mol) and decrease in the Se-Ge bonds (49.42 kcal/mol) with the addition of Pb. Also the heat of atomization value of lead (Pb) is less than that of Ge and hence the final heat of atomization of the system decreases. This decrease in the average single bond energy with the increase in lead content may also cause the decrease in energy band gap. Bond energy of heteropolar bonds can be calculated by using the following equation suggested by Pauling[21]:

$$E_{A\text{-}B} = [E_{A\text{-}A} \,.\, E_{B\text{-}B}]^{0.5} + 30\,[\chi_A - \chi_B]^2 \quad \ldots (12)$$

where $E_{A\text{-}B}$ is the bond energy of heteropolar bonds and E_{A-A}, E_{B-B} are the bond energies of homopolar bonds. χ_A and χ_B are the electronegativites of A and B elements, respectively. According to chemical bond approach (CBA), heteropolar bonds form more easily than the homopolar bonds. The different possible homopolar bonds formed in the composition are; Se-Se = 44 kcal/mol, Te-Te = 33 kcal/mol, Ge-Ge = 37.60 kcal/mol and Pb-Pb = 20.48 kcal/mol. The electronegativity values for Se, Te, Ge and Pb according to the Pauling scale are 2.55, 2.10, 2.01 and 2.33, respectively[21]. Consequently, using Eq. (12), the bond strength of heteropolar bonds is; Se-Te=44.18 kcal/mol, Se-Ge=49.42 kcal/mol and Se-Pb=31.47 kcal/mol. The bond formation takes place according to decrease in their bond energies. The chemical bond distribution of possible bonds is given in Table 3. Se-Ge bonds take place firstly which are accompanied by Se-Te bonds, then Se-Pb bonds and hence lastly homopolar Se-Se bonds are formed.

Cohesive energy is the energy required to break all the bonds associated with the constituent atoms. The chemical bond approach (CBA) is used to calculate the cohesive energy of the investigated material[22]. Cohesive energy is calculated by adding the bond energies of all the expected bonds in the material:

$$CE = \sum C_i E_i \quad \ldots (13)$$

where C_i and E_i are the number of expected chemical bonds and energy of each corresponding bond, respectively. Cohesive energy is the stabilization energy of the immense bunch of material per atom. Calculated values of *CE* along with the distribution of chemical bonds and energy gap values are given in Table 3. Cohesive energy of the composition

Table 2 — Values of mean bond energy, heat of atomization, average single bond energy, glass transition temperature for $(Se_{80}Te_{20})_{94-x}Ge_6Pb_x$ (x = 0, 2, 4, 6, 8 and 10).

Composition	<*E*> (eV/atom)	H_s (kJ/mol)	H_s/Z	T_g (K)	
				Tichy-Ticha	Experimental
$(Se_{80}Te_{20})_{94}Ge_6$	2.016	230.36	108.66	347.07	362.04
$(Se_{80}Te_{20})_{92}Ge_6Pb_2$	2.004	229.84	106.40	343.34	357.50
$(Se_{80}Te_{20})_{90}Ge_6Pb_4$	1.995	229.32	104.23	341.45	351.83
$(Se_{80}Te_{20})_{88}Ge_6Pb_6$	1.990	228.80	102.14	340.00	347.16
$(Se_{80}Te_{20})_{86}Ge_6Pb_8$	1.989	228.28	100.12	339.17	-
$(Se_{80}Te_{20})_{84}Ge_6Pb_{10}$	1.988	227.76	98.17	338.36	-

Table 3 — Possible dispersal of bonds, cohesive energy and E_g for $(Se_{80}Te_{20})_{94-x}Ge_6Pb_x$ (x = 0, 2, 4, 6, 8 and 10).

Composition	Possible dispersal of bonds				CE (kcal/mol)	E_g (eV)
	Se-Te	Se-Ge	Se-Pb	Se-Se		
$(Se_{80}Te_{20})_{94}Ge_6$	0.25	0.159	-	0.590	45.00	1.58
$(Se_{80}Te_{20})_{92}Ge_6Pb_2$	0.25	0.163	0.054	0.533	44.24	1.55
$(Se_{80}Te_{20})_{90}Ge_6Pb_4$	0.25	0.166	0.111	0.472	43.55	1.52
$(Se_{80}Te_{20})_{88}Ge_6Pb_6$	0.25	0.170	0.170	0.409	42.83	1.49
$(Se_{80}Te_{20})_{86}Ge_6Pb_8$	0.25	0.174	0.233	0.343	42.08	1.46
$(Se_{80}Te_{20})_{84}Ge_6Pb_{10}$	0.25	0.178	0.297	0.274	41.28	1.43

decreases with Pb content. This may be attributed to the replacement of stronger Se–Ge bonds (49.42 kcal/mol) by the weaker Pb–Se bonds (31.47 kcal/mol). Moreover the bond formations with lead are slightly ionic in nature and provide ionic character to the material. This weakens the network and makes the structure delicate.

The energy gap values for $(Se_{80}Te_{20})_{94-x}Ge_6Pb_x$ (x = 0, 2, 4, 6, 8 and 10) nano-composites are calculated theoretically[23] using the band gap values for individual atom in the composition as Se = 1.95 eV, Te = 0.335 eV, Ge = 0.95eV and Pb = 0 eV. The decrease in cohesive energy decreases the energy of conduction band edge that causes a decrease in the band gap between bonding and antibonding orbitals and hence optical energy gap decreases[24]. Also the overall decrease in the energy of the system is responsible for the decrease in energy gap. Obtained energy gap values are given in Table 3.

The structural examination of the investigated alloys indicates that the addition of Pb to the parent ternary $(Se_{80}Te_{20})_{94}Ge_6$ alloy made it nano-crystalline in nature and this may be due to the metallic nature of lead. The theoretical investigations indicate that the average co-ordination number and hence number of constraints increase with the increase in Pb content. Since lead is four fold co-ordinated and is also a heavy element, therefore, there is increase in density, rigidity, strength and hence average co-ordination number increases. The number of lone pair electrons which is calculated by subtracting the average co-ordination number from valence electrons. With the increase in Pb at.wt.%, the interaction diminished the role of lone -pair electrons in the formation of glass. L lies between 3.36 and 3.76 for the investigated alloys, which is much greater than the criterion proposed by Zhenhua for a good glass former. It is found that mean bond energy (Table 2) decreases with increasing Pb content. Similar behaviour is observed for T_g as they are directly proportional to each other. Also the bond energy of heteropolar (Se-Pb) bonds are much smaller than the bond energy of replaced (Se-Se) bonds, which as a whole leads to the decrease in the mean bond energy of the composition and hence the glass transition temperature. The heat of atomization is also found to decrease with Pb concentration because the H_s for Pb value is less as compare to the heat of atomization for Se, Te and Ge. So there is a decrease in the overall value of heat of atomization and hence average single bond energy also decreases. There is decrease in energy gap with Pb amount, which can be correlated to the decrease in average single bond energy and it can also be linked to the decrease in overall bond energies. The decrease in energy gap may also be associated with the decrease in cohesive energy.

4 Conclusions

In the present study, the structural characterization and the different physical properties viz average co-ordination number, number of constraints, lone pair electrons, fraction of floppy modes, heat of atomization, cohesive energy, mean bond energy, glass transition temperature and energy band gap are deduced for new quaternary $(Se_{80}Te_{20})_{94-x}Ge_6Pb_x$ (x = 0, 2, 4, 6, 8 and 10) chalcogenide nano-composites. Nano particle size of Pb additive Se-Te-Ge alloys was deduced using the XRD and is further confirmed by FESEM. Addition of Pb content to the Se-Te-Ge system increases the average co-ordination number and number of constraints, whereas, all the other investigated parameters show a reverse trend. Cohesive energy is calculated by using the CBA model and is found to decrease with the increase in Pb content. Glass transition temperature is deduced theoretically by using Tichy-Ticha approach and is found to be in concordance with the experimental values.

References

1 Stender C L, Sekar P & Odom T W, *J Solid State Chem*, 181 (2008) 1621.
2 Khan S A, Al-Agel F A & Al-Ghamdi A A, *Superlattices Microstuct*, 47 (2010) 695.
3 Adachi T, Tanaka A, Hasegawa Y & Kawai T, *Thin Solid Films*, 516 (2008) 2460.
4 Pinkas J, Reichlova V, Zboril R, Moravec Z, Bezdicka P & Matejkova J, *Ultrason Sonochem,* 15 (2008) 257.
5 Patial B S, Thakur N & Tripathi S K, *Phys Scripta*, 85 (2012) 045603.
6 Concha B M, Biasi E D & Zysler R D, *Phyisca B*, 403 (2008) 390.
7 Ibrahim M M, Saleh SA, Ibrahim E M M & Abdel Hakeem AM, *J Alloys Compd*, 452 (2008) 200.
8 Qing L, Ding Y, Shao M, Wu J, Yu G & Qian Y, *Mater Res Bull*, 38 (2003) 539.
9 Dashevsky Z, Shusterman S, Dariel M P & Drabkin I, *J Appl Phys*, 92 (2002) 1425.
10 Anjali, Patial B S, Bhardwaj S, Awasthi A M & Thakur N, *Physica B*, 523 (2017) 52.
11 Patial B S, Neha Thakur N & Tripathi S K, *Int J Adv Res Phys Sci*, 1 (2014) 9.
12 Thorpe M F, *J NonCryst Solids*, 57 (1983) 355.
13 Fouad S S, El-Bana M S, Sharma P & Sharma V, *Appl Phys A*, 120 (2015) 137.
14 Singh D, Kumar S & Thangaraj, *Adv Appl Sci Res*, 2 (2011) 20.

15 Phillips J C & Thorpe M F, *Solid State Commun*, 53 (1985) 699.
16 Zhenhua L, *J Non-Cryst Solids*, 127 (1991) 298.
17 Tichy L & Ticha H, *Mater Lett*, 21 (1994) 313.
18 Patial B S, Thakur N & Tripathi S K, *Thermochim Acta*, 513 (2011) 1.
19 Tichy L & Ticha H, *J Non-Cryst Solids*, 189 (1995) 141.
20 Sadagopan V & Gatos H C, *Solid State Electron*, 8 (1965) 529.
21 Pauling L, *The nature of the chemical bond and the structure of molecules and crystals*, (Cornell University Press: New York), 1960.
22 Cox J D, Wagman D D & Medvedev V A, *CO - DATA key values for thermodynamics*, (Hemisphere Publishing Corp: New York), 1989.
23 Pattanaik A K & Srinivasan A, *Semicond Sci Technol*, 19 (2004) 157.
24 Dashan A & Aly K, *Philos Mag*, 88 (2008) 361.